GEOPHYSICS, VOL. 71, NO. 4 (JULY-AUGUST 2006); P. R49–R58, 13 FIGS., 2 TABLES.
10.1190/1.2204964

# Fast simulated annealing inversion of surface waves on pavement using phase-velocity spectra

Nils Ryden[1] and Choon Byong Park[2]

## ABSTRACT

The conventional inversion of surface waves depends on modal identification of measured dispersion curves, which can be ambiguous. It is possible to avoid mode-number identification and extraction by inverting the complete phase-velocity spectrum obtained from a multichannel record. We use the fast simulated annealing (FSA) global search algorithm to minimize the difference between the measured phase-velocity spectrum and that calculated from a theoretical layer model, including the field setup geometry. Results show that this algorithm can help one avoid getting trapped in local minima while searching for the best-matching layer model. The entire procedure is demonstrated on synthetic and field data for asphalt pavement. The viscoelastic properties of the top asphalt layer are taken into account, and the inverted asphalt stiffness as a function of frequency compares well with laboratory tests on core samples. The thickness and shear-wave velocity of the deeper embedded layers are resolved within 10% deviation from those values measured separately during pavement construction. The proposed method may be equally applicable to normal soil site investigation and in the field of ultrasonic testing of materials.

## INTRODUCTION

Pavement is typically constructed using a stiff top layer of asphalt or concrete over a compacted base layer of granular or stabilized material (Figure 1). The bearing capacity and durability of the pavement depend on the stiffness of these layers. It is therefore very valuable to be able to determine the properties of the layers nondestructively. Nondestructive testing (NDT) of pavement based on surface waves may obtain both the thickness and stiffness properties of the pavement layers. With an efficient NDT technique these properties can be mapped as a function of time and space, providing a valuable tool in pavement design and management. Since early studies by Jones (1962) and Vidale (1964), surface-wave methods have been recognized as a promising approach for seismic/acoustic NDT of pavement. The spectral analysis of surface waves (SASW) method (Heisey et al., 1982; Nazarian, 1984; Stokoe et al., 1994) is now widely used, and field protocols for pavement design and maintenance based on seismic methods are being developed (Haegeman, 2002; Abdallah et al., 2003; Ekdahl et al., 2004). The thickness and stiffness of the top layer are the most efficient and accurate properties to evaluate (Roësset et al., 1990; Akhlaghi and Cogill, 1994). The inversion for properties of deeper embedded layers has been the most challenging part of surface-wave testing of pavement (Ganji et al., 1998; Gucunski et al., 2000). The embedded second layer (base) underneath the asphalt layer has been particularly difficult to resolve (Aouad, 1993; Wu et al., 2002).

Studies by Ryden et al. (2004) and Ryden and Lowe (2004) show that guided wave propagation in pavement structures is more complicated than previously addressed, particularly with the issue of multiple modes of leaky waves with large variations in excitability between different modes. Traditional surface-wave methods based on a single composite dispersion curve may therefore not be sufficient to resolve adequately the dispersion properties from pavement systems. On the other hand, the multichannel approach has proved to be capable of separating different modes of surface waves (Gabriels et al., 1987; Park et al., 1999; Ryden et al., 2004). In this study a synthetic source array with only one receiver (accelerometer) is used to record a multichannel equivalent data set. The receiver is fixed at a surface point and receives signals $u(t)$ from several hammer impacts at incremental offsets $x$ (Ryden et al., 2001, 2004). All recorded signals are then compiled to make an equivalent multichannel record $u(x,t)$ for dispersion analysis. A schematic of the field setup over typical pavement construction is shown in Figure 1.

Inversion of surface-wave dispersion curves is a nonunique and nonlinear inverse problem where a direct solution is impossible. The conventional inversion technique for surface-wave methods is usually based on a linearized damped least-squares solution, driven by partial derivatives of each inverted parameter (Jacobian matrix)

Manuscript received by the Editor June 3, 2004; revised manuscript received December 14, 2005; published online July 5, 2006.
[1]Lund University, Department of Engineering Geology, Box 118, SE-221 00 Lund, Sweden. E-mail: nils.ryden@tg.lth.se.
[2]University of Kansas, Kansas Geological Survey, 1930 Constant Avenue, Lawrence, Kansas 66047-3726. E-mail: park@kgs.ku.edu.

(Menke, 1989; Xia et al., 1999). The multimodal nature of surface-wave data from pavement (Ryden and Lowe, 2004; Ryden and Park, 2004) makes the partial derivative approach difficult because the measured apparent dispersion curve jumps between mode branches and the partial derivatives are not sufficiently stable (Foti et al., 2003). When discrete dispersion curves are inverted, the correct mode-number identification also becomes a critical and difficult task (Socco et al., 2002; Beaty and Schmitt, 2003; Zhang and Chan, 2003). Forbriger (2003) presents a gradient-based inversion procedure of the complete wavefield spectrum to solve the problems with mode-number identification. A general problem with linearized gradient-based inversion techniques applied to nonlinear and nonunique problems is that the solution is often dependent on the starting model and may not always converge to the global minimum of the objective function (Sen and Stoffa, 1995). In the case of pavement systems, the problem is further complicated by highly variable parameter sensitivities and correlated parameters. These difficulties are the main motivation of our study.

The proposed method is based on a global search algorithm, fast simulated annealing (FSA) (Szu and Hartley, 1987), which finds the best possible match between the measured and the modeled complete phase-velocity spectrum of surface waves. With this procedure, data reduction and the extraction of an experimental dispersion curve are avoided. This study was initiated by the complicated nature of wave propagation in pavement structures. However, the same procedure can be used for the inversion of surface wave data from soil sites or in the field of ultrasonic testing of composite plates and coatings.

## PHASE-VELOCITY SPECTRA

Figure 2 shows an example of a typical phase-velocity spectrum recorded over three-layer pavement constructed in Malmoe, Sweden. Data were collected with 0.05 m station separation over an offset range from 0.05–5.00 m using a small hammer (source) and one accelerometer (receiver), as illustrated in Figure 1. The grayscale image shows normalized summed amplitudes as a function of frequency and phase velocity (Park et al., 1998). Over the full-frequency range (Figure 2a), most energy is concentrated along the fundamental-mode antisymmetric Lamb-wave dispersion curve *A*0, which corresponds to the top layer acting as a free plate (dashed line). The symmetric Lamb-wave mode *S*0 (dotted line) is visible in a limited frequency range — here, 8–10 kHz at 3500 m/s (Ryden and Park, 2004). This portion of the *S*0 mode corresponds to the first-arrival wave in the time domain, i.e., all measurable types of waves in this layer setting and frequency range are guided. Figure 2b shows detectable mode branches at lower frequencies. The pattern of these mode branches is a function of the pavement-layer properties (Ryden and Lowe, 2004).

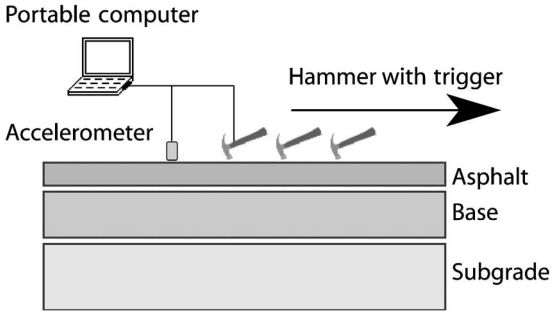


Figure 1. Schematic of typical pavement construction and field setup geometry using only one receiver and one source.

## Measured phase-velocity spectrum

The measured phase-velocity spectrum is obtained automatically from multichannel surface-wave data using the plane-wave transformation technique of Park et al. (1998, 1999). The multichannel equivalent record compiled from measurements at different offsets $u(x,t)$ is transformed to the frequency–phase-velocity domain using

$$S(\omega, c_T) = \int e^{-i(\omega/c_T)x} U(x,\omega)dx, \qquad (1)$$

where $U(x,\omega)$ is the normalized complex spectrum obtained from the Fourier transformation of $u(x,t)$, $\omega$ is the angular frequency, $c_T$ is the testing-phase velocity, and $S(\omega,c_T)$ is the slant-stack amplitude for each $\omega$ and $c_T$, which can be viewed as the coherency in linear arrival pattern along the offset range for that specific combination of $\omega$ and $c_T$. When $c_T$ is equal to the true phase velocity of each frequency component, there is a maximum in $S(\omega,c_T)$. Calculating $S(\omega,c_T)$ over the frequency and phase-velocity range of interest generates the phase-velocity spectrum where dispersion curves can be identified as high-amplitude bands. Note that $U(x,\omega)$ is normalized in both the $x$ and $\omega$ dimensions, so all amplitudes at different frequencies and distances have unit amplitude but with preserved phase information. This processing scheme resolves phase velocity better than conventional frequency-wavenumber ($f$–$k$) and time-phase ($\tau$–$p$) transformations (Beaty et al., 2002; Dal Moro et al., 2003), particularly when a limited number of signals (traces) are used (Dal Moro et al., 2003).

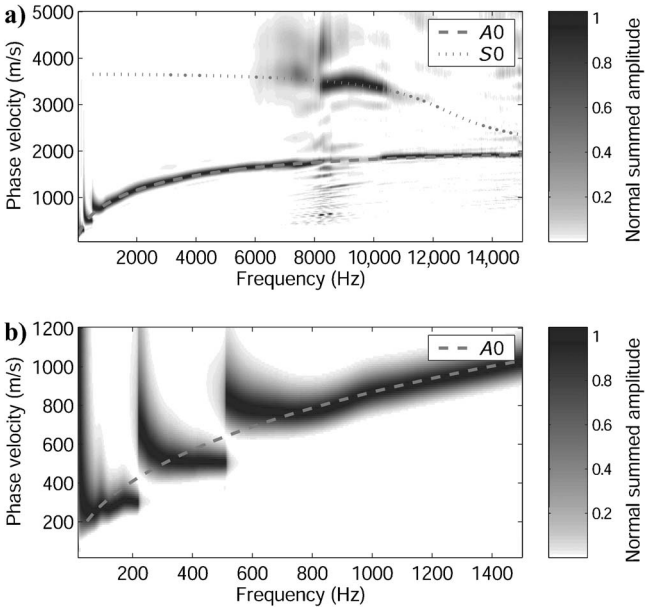


Figure 2. (a) Gray scaling corresponding to the measured phase-velocity spectrum from a three-layer pavement constructed in Malmoe, Sweden. Predicted Lamb-wave dispersion curves from the top layer, modeled as a free plate, are superimposed as dashed (*A*0) and dotted (*S*0) lines. (b) The same measured data set displayed in a lower frequency and phase-velocity range, showing branches of dispersion curves.

A detailed parametric examination of equation 1's resolution in response to its parameters is presented by Park et al. (2001).

## Theoretical phase-velocity spectrum

The theoretical phase-velocity spectrum (forward model) is calculated from a known layer model **m** and the field setup geometry. The forward model ideally should mimic the field setup and measured response as closely as possible to generate a phase-velocity spectrum that is directly compatible with the measured replica. Therefore, the receiver and source locations are also included in the forward model so that superposition of different modes of propagation can be accounted for.

The first step in the forward model is to find the resonant wavenumbers $k$ (modes) at the surface of **m** resulting from a vertical-point load. The stiffness matrix approach by Kausel and Roësset (1981) is used for this calculation. The stiffness matrix approach relates loads $p$ and displacements $U$ at the layer interfaces in the $\omega$–$k$ domain. Each layer is assumed to be homogeneous, with thickness $h$ and material properties defined by the shear-wave velocity $V_S$, Poisson's ratio $\nu$, and bulk density $\rho$. The basic equations originate from the transfer matrix method (Thomson, 1950; Haskell, 1953) but are rearranged to be expressed in loads instead of partial wave amplitudes. All layer equations are omitted here but can be found along with more details in Kausel and Roësset (1981), Gucunski and Woods (1992), and Gucunski and Maher (2000).

The stiffness matrix method is usually implemented along with complex bulk wave velocities where the complex part is addressed as material damping. With this approach $k$ is always complex and there is less risk of numerical instabilities. Alternatively, a small damping coefficient can be added as a complex component of each $k$, in which case a reasonable amount of leakage into the half-space can be accounted for implicitly (Ryden and Lowe, 2004). When all layer matrices are assembled, vertical amplitudes at the surface $U$ can be calculated for each frequency and wavenumber of interest. By scanning through a range of testing-phase velocities at each frequency, resonant peaks can be extracted along with their relative amplitude ratios. Figure 3a shows the surface response from a vertical unit load as a function of $c_T$ at 760 Hz calculated from the reference layer model in Table 1. Two resonant phase velocities (wavenumbers $k = \omega/c$) can be identified with a relative amplitude ratio of 0.85. These resonant wavenumbers are not necessarily the fundamental and the first higher mode. An exact mode-number identification is not necessary because the inversion is based on the phase-velocity spectrum instead of discrete dispersion curves.

In the next step the extracted modes $U_{\text{pred}}(\omega,k)$ are superimposed on the same offset range as used for the measured data. The Hankel function is used instead of the plane-wave approximation to account for cylindrical spreading. This introduces a nonlinear phase shift at near offsets and, to a certain degree, accounts for the near-field effect (Zywicki, 1999). The relative phase lag at each offset can be expressed with a complex spectrum using

$$U_{\text{pred}}(x,\omega) = qR\int_0^\infty J_1(kR)J_0(kx)U_{\text{pred}}(\omega,k)dk, \qquad (2)$$

calculated by using numerical integration, where $R$ represents the radius of the source point, $q$ is the load intensity, and $J_0$ and $J_1$ are Bessel functions of the first kind of orders 0 and 1, respectively. In this application we use $R = 0.005$ m and $q = 1$, but these values are not critical since the radius of the source point is much smaller than the wavelengths of interest and amplitudes are normalized in the subsequent processing of $U_{\text{pred}}(x,\omega)$. The resulting phase angle as a function of offset is plotted in Figure 3b. The superposition of two different phase velocities at the same frequency creates a nonlinear phase-offset pattern. This nonlinear phase-offset curve is typical in surface-wave testing of pavement and was documented by Van der Poel (1951) more than 50 years ago.

In the final step of the forward model, the theoretical complex spectrum obtained from equation 2 is transformed to the frequency-phase velocity domain using equation 1. Now a predicted phase-velocity spectrum $S_{\text{pred}}(\omega,c_T,\mathbf{m})$ is generated that can be compared directly to the observed $S_{\text{obs}}(\omega,c_T)$ obtained from the measured field data. Figure 3c shows this phase-velocity spectrum at 760 Hz. The difference between Figures 3a and 3c is important for the subsequent inversion procedure. Figure 3c is offset dependent and includes modal superposition effects that are not present in Figure 3a.

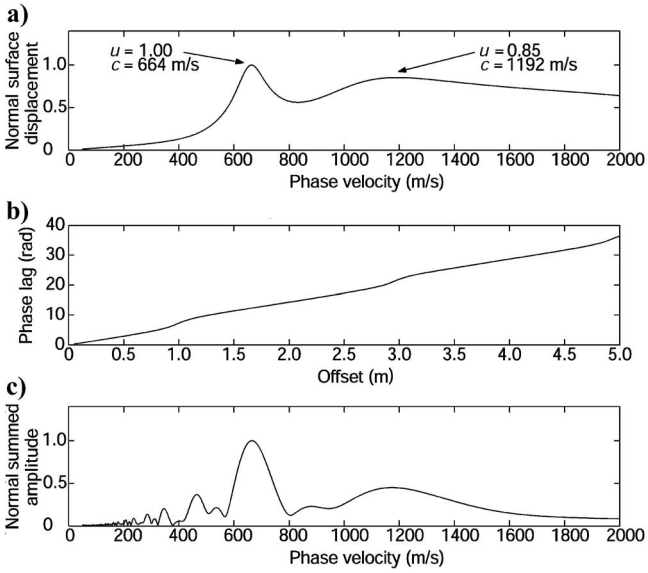


Figure 3. (a) Surface displacement at 760 Hz from a vertical unit load at the surface of the synthetic layer model (Table 1), showing two different modes of propagation (peaks). (b) The resulting phase-offset curve and the typical steplike behavior created by the interference of two different modes. (c) The corresponding summed amplitude spectrum generated from the multichannel analysis of surface waves (MASW) transformation technique.

**Table 1. Synthetic three-layer model, with equivalent values obtained by inversion in parentheses.**

| Layer | $h$ (m) | $\nu$ | $\rho$ (kg/m$^3$) | $V_S$ (m/s) |
|---|---|---|---|---|
| 1 | 0.220(0.224) | 0.350 | 2000.0 | 1400.0(1401.5) |
| 2 | 0.400(0.404) | 0.350(0.349) | 2000.0 | 300.0(303.0) |
| 3 | ∞ | 0.350 | 2000.0 | 100.0(103.4) |

## SENSITIVITY ANALYSIS OF LAYER PARAMETERS

The predicted phase-velocity spectrum is compared to the observed phase-velocity spectrum through the objective function

$$M(\mathbf{m}) = \left( 1 - \frac{\sum_{y=1}^{K} \sum_{z=1}^{N} |\mathbf{S}_{yz,\mathrm{obs}}| \cdot |\mathbf{S}_{yz\ \mathrm{pred}}|}{\sum_{y=1}^{K} \sum_{z=1}^{N} |\mathbf{S}_{yz,\mathrm{obs}}|^2} \right), \qquad (3)$$

where $M$ represents the mismatch between the two phase-velocity spectra. The summation along $y$ and $z$ represents a summation along frequency and phase velocity, respectively, in the phase-velocity spectrum. The value of $M$ can lie between 0 and 1, where 0 represents a perfect match (this value is minimized in the subsequent inversion procedure). In this study, amplitudes in both the predicted and observed phase-velocity spectra are raised to an arbitrary power of three to suppress low amplitudes and to increase the sharpness of the main amplitude bands (dispersion curves).

It is essential to find out which parameters in the layer model have a noticeable influence on the phase-velocity spectrum. Therefore, we first present a sensitivity analysis. The layer model in Table 1 represents a reference pavement layer model. The 1D $M$ functions are calculated by scanning through a range of parameter values ±50% compared to the true values of the reference layer model, keeping all other layer parameters fixed. The corresponding 1D mismatch functions of the most sensitive parameters are presented in Figure 4. This plot can be viewed as a 1D sensitivity analysis to each parameter in the reference layer model. In this case, the sensitivity (sharpness and depth of the valley at the true value) to each parameter is influenced by a number of parameters, such as the specific reference layer model, frequency range, phase-velocity range, and offset range. The frequency range and frequency sampling (e.g., linear, logarithmic, or other) have the largest influence on the $M$ value. In general a denser sampling and higher maximum frequency result in larger sensitivities. However, in practice, real data are always contaminated with noise, and there will be a maximum frequency above which mode branches cannot be resolved individually (e.g., at about 1000 Hz in Figure 2b). In this sensitivity example the minimum and maximum frequencies are 60 and 1000 Hz, respectively, with a linear sampling of 100 values. The modeled offset range is 0.05–5.00 m with a station separation of 0.05 m. Figure 4 shows that the phase-velocity spectrum used in this test is most sensitive to the thickness and shear-wave velocity of the second layer. However, Poisson's ratio of the second layer also shows a noticeable influence on the phase-velocity spectrum.

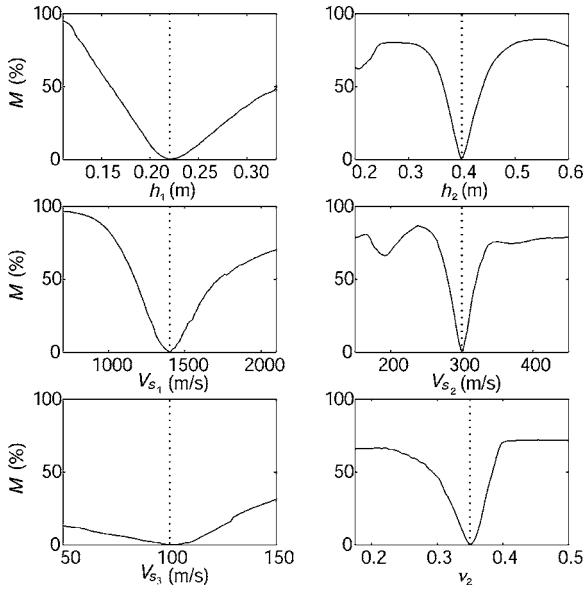


Figure 4. 1D cross sections of the parameter space, showing the variation in sensitivity of different parameters of the layer model. The dotted line corresponds to the true value of each parameter (Table 1).

Although numeric results such as these are model dependent, we can conclude that both the thickness and the shear-wave velocity of each layer should be estimated meaningfully through the inversion procedure. However, further difficulties can arise from correlated parameters and/or many local minima within the parameter space. The shape of the $M$ function for each parameter reveals some of these difficulties (Figure 4). Unfortunately, this type of plot only gives a 1D picture of the complete multidimensional parameter space. In Figure 5, 2D $M$ functions of selected parameters are plotted. The global minimum is marked with a white asterisk, and local minima are marked with black dots. Some of the features that make the inversion of pavement layer properties a challenging task now become highly visible, i.e., local minima and correlated parameters. These features are typical for this problem and show why a global optimization technique is necessary for the inversion of surface-wave data containing multiple mode branches.

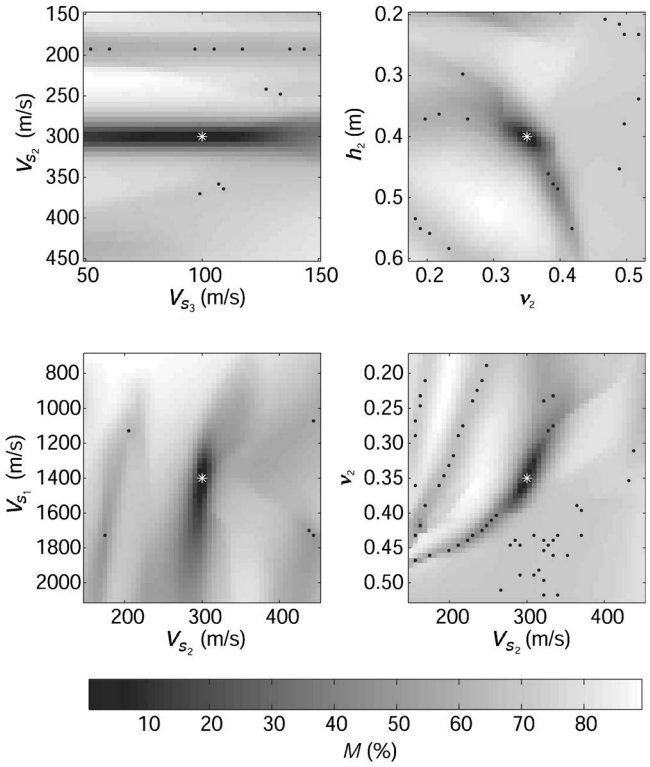


Figure 5. 2D cross sections of the parameter space grayscaled with respect to the mismatch $M$ value. Dark gray corresponds to low $M$ values, and the white asterisk shows the true parameter value (global minimum). Local minima are marked with black dots.

## INVERSION BY FSA

The goal of the inversion procedure is to find a layer model whose corresponding phase-velocity spectrum matches the measured spectrum best. This case represents the global minimum of the objective function (equation 3). A number of search strategies for this type of problem have been presented (Mosegaard and Sambridge, 2002). A straightforward approach is to define reasonable upper and lower bounds for each parameter to invert for and then to scan through all trial layer models $\mathbf{m}_j$ in the search for the global minimum. If each parameter is divided into $N$ intervals and there are $Z$ numbers of parameters to invert for, the complete parameter space can be divided into $N^Z$ trial layer models. Unfortunately, this approach is impractical for large numbers of $N$ and $Z$. This is our main motivation for using statistical search strategies instead. Simulated annealing (SA) is a global direct Monte Carlo method (Kirkpatrick et al., 1983; Laarhoven and Aarts, 1987) especially developed to find the global minimum of challenging functions with many local minima. The method has been applied to surface-wave inversion in previous studies where discrete continuous dispersion curves have been matched successfully (Martínez et al., 2000; Beaty et al., 2002; Hadidi and Gucunski, 2003). Now we apply the SA concept to the inversion of phase-velocity spectra in place of discrete dispersion curves. Note that SA is only one of several global optimization methods; new methods are being developed continuously (see, for example, Sambridge, 1999).

### Simulated annealing

The SA method is based on a random walk in the parameter space in combination with the Metropolis criterion (described later), intended to find the global minimum of challenging functions with many local minima. This process originates from the natural optimization process of thermodynamic annealing in crystalline solids (Laarhoven and Aarts, 1987). The search strategy involves two control parameters whose values need to be set subjectively: an initial temperature $T_0$ with the same unit as the objective function and a cooling parameter $a$. Each iteration $j$ involves a random perturbation of each parameter in $\mathbf{m}$ followed by a forward model and mismatch calculation. The initial model is drawn randomly from the predefined interval $\Delta m_l$ of each parameter $l$. If the calculated mismatch is smaller than that for the previously accepted model, the new model is accepted as a transition $i$. However, if the mismatch is larger than it was for the previous model, the new model may be accepted if

$$r < e^{-\Delta M/T}, \tag{4}$$

where $r$ is a random number from 0 to 1, $\Delta M$ is the mismatch difference between the current and the previously accepted models, and $T$ is the current temperature that is decreased with the number of accepted transitions $i$ according to the chosen cooling schedule. This second chance of acceptance (known as the Metropolis criterion) is the key concept of the SA algorithm and can make the search expand from a local minimum to a global minimum. Figure 6 shows a process map of the SA algorithm used in this study.

Cooling schedule and perturbation size are the most important parameters to optimize for each specific SA application. A common cooling schedule is the exponential

$$T = T_0 a^i, \tag{5}$$

where the cooling parameter $a$ is a number smaller than one. Control parameters $T_0$ and $a$ need to be chosen subjectively. Initially, the temperature should be set high enough so that many iterations $j$ (about 90%, according to Dosso et al., 2001) are accepted as transitions $i$. After a preset number of transitions, the temperature should be reduced gradually according to the cooling parameter. The effect of $a$ decreases the probability of equation 4 being satisfied with the number of accepted transitions, so the algorithm eventually converges to a minimum. If the control parameters $a$ and $T_0$, whose values are usually application dependent, are set properly for the specific application, there should be a good chance of finding the global minimum. However, there is no guarantee that the global minimum has been found. Several researchers present techniques for finding the optimum cooling schedule (Basu and Frazer, 1990; Hoffmann and Salamon, 1990; Andresen and Gordon, 1994).

The difference between standard SA and FSA (Szu and Hartley, 1987) lies in the way the new models are perturbated randomly for each new iteration. If the search range $\Delta m_l$ assigned to each parameter being inverted is too large, the process will waste a lot of time at low temperatures where large perturbations are not likely. Therefore, the FSA method involves a temperature-scaled Cauchy distribution of the perturbation of each parameter (Sen and Stoffa, 1995). The Cauchy distribution has a narrow central peak and wide tails, providing concentrated local sampling in combination with occasional large perturbations. After each accepted transition, each parameter $m_l$ is perturbed to obtain a new test value $m_l'$ according to

$$m_l' = m_l + \Delta m_l \left(\frac{T}{T_0}\right)\left(\eta_1 \tan\left(\frac{\eta_2 \pi}{2}\right)\right), \tag{6}$$

where $\eta_1$ and $\eta_2$ are uniform random variables on $[-1,1]$ and $\Delta m_l$ are the predefined search intervals for each parameter $l$. With the

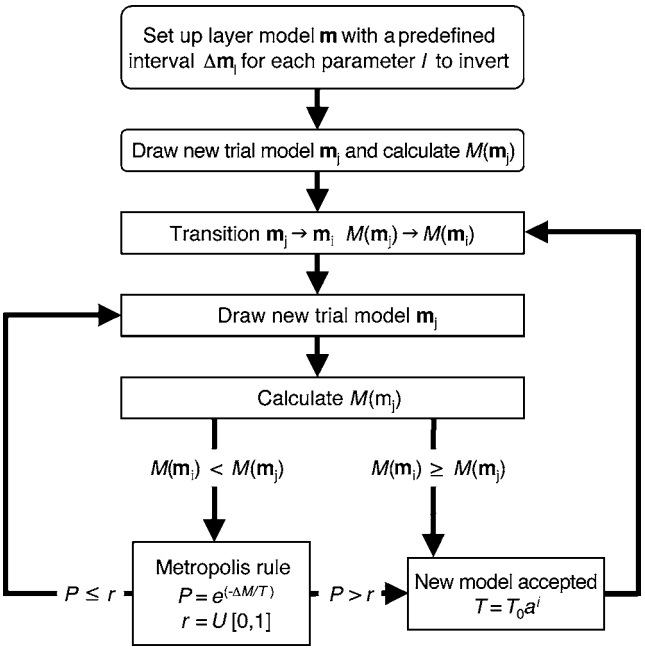


Figure 6. Flowchart of the simulated annealing algorithm. Index $i$ represents the number of accepted transitions, and index $j$ represents the total number of iterations.

FSA approach, all parameters are perturbed at once after each iteration $j$; standard SA algorithms typically perturb one parameter at a time and cycle through all parameters (Laarhoven and Aarts, 1987). Perturbing all parameters at once is more effective for problems with correlated parameters (Dosso et al., 2001).

## SYNTHETIC DATA TEST

We first demonstrate our proposed inversion procedure on synthetic data from the reference layer model (Table 1). The FSA schedule was set up with five transitions per temperature and an exponential cooling schedule with $T_0 = 30$ and $a = 0.99$. These values are a good compromise between a fine search and computational time for this specific problem. Parameter values and corresponding $M$ values from all iterations used for the inversion are plotted in Figure 7. The predefined search range of each parameter is equal to the horizontal axis range in Figure 7. The dashed lines indicate the true values from Table 1. Figure 7 shows how the FSA algorithm searches through the given range of parameter values and finally converges toward the true values. The width of the peak of all dots in the figure indicates the multidimensional sensitivity of each parameter. Note that the shape of the distribution of all dots in Figure 7 includes the multidimensional sensitivity of each parameter, while Figure 4 only shows a 1D picture of the parameter space.

The inversion algorithm was set to stop after 700 transitions or an $M$ value lower than 0.400%. In this example, an $M$ value of 0.327% was reached after 457 transitions and 9095 iterations. The target and the best-matching phase-velocity spectrum are plotted in Figure 8 along with a difference plot between the two. The inversion of this synthetic data test could have continued to run for even lower $M$ values, possibly resulting in inverted values even closer to the reference values. However, in practice real data are contaminated with noise, and these small variations in the $M$ value may not be realistic.

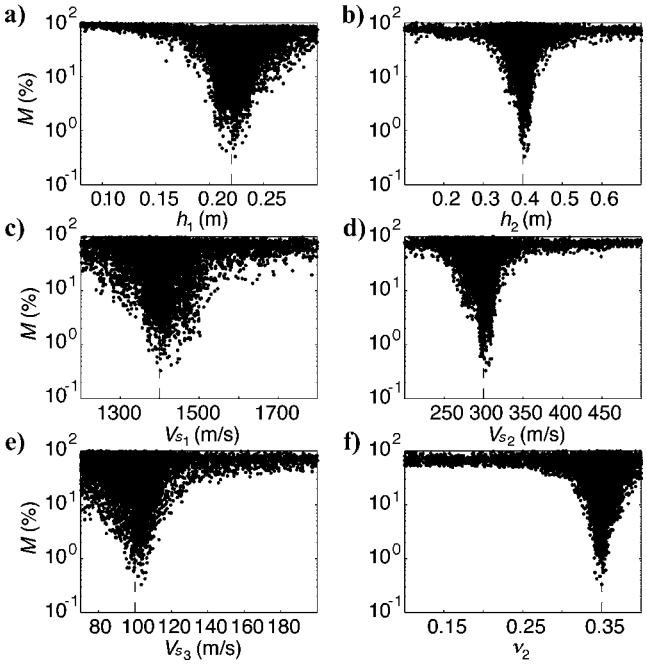


Figure 7. Mismatch as a function of parameter value from the inversion of the synthetic data test shown by dots. Dashed lines show the true values.

The final inverted parameter values are given in parentheses in Table 1. These values represent the dots with the lowest $M$ values from Figure 7. The shear-wave velocity of the half-space $V_{S3}$ shows the largest deviation from the true value, with an error of 3.4%. The other five parameters are all well resolved within about 1% of the true values. The thickness of the second layer $h_2$ shows a sharp peak in Figure 7b, which indicates the parameter is well resolved, although this layer parameter has been the most difficult to invert with conventional methods.

## FIELD-DATA TEST

The inversion procedure is tested on real field data from a pavement construction site in Malmoe, Sweden. The given layer model at the test site is presented in Table 2. The thickness of each layer is accurately measured and controlled during pavement construction and the values in Table 2 can be considered true reference values. Accurate in-situ reference shear-wave velocities from the embedded layers in pavement construction are more difficult to obtain. To collect the best possible reference data, measurements were taken on top of each layer during construction. These measurements were made with 0.10 m station separation over an offset range from 0.10–4.00 m using a small hammer (source) and one accelerometer (receiver). With a laptop-based data acquisition system, this type of 40-station walkaway record was collected in approximately 10 minutes. An 80-ms record length and 100-kHz sampling rate were used. Data from the top of the subgrade (clay till) are shown in Figure 9. Each trace is normalized and plotted as a wiggle trace with filled positive amplitudes. The best-matching P-wave velocity is indicated with a dotted line in Figure 9a. At this site, the clay till layer is more than 5.0 m thick and is homogeneous. As seen in both Figures 9a and b, high-frequency (100–500 Hz) surface waves are almost nondispersive, with a velocity of about 200 m/s. In this frequency range the wavelength is shorter than the layer thickness, so the phase velocity can be assumed to represent the surface-wave velocity $V_R$ of

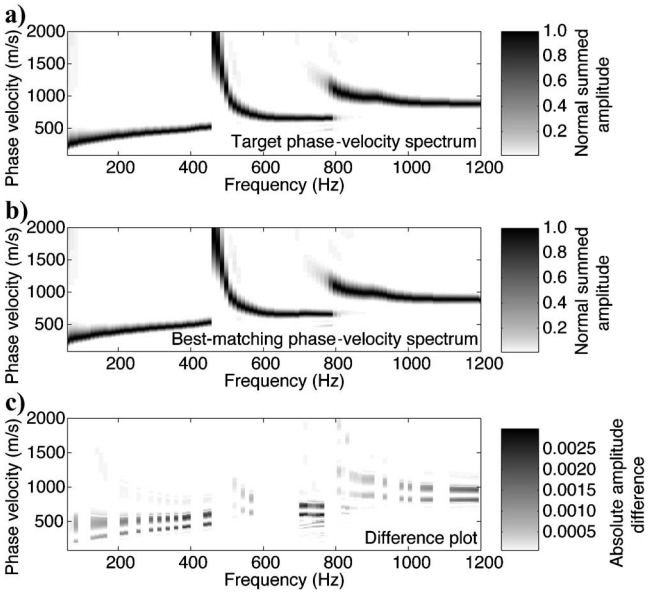


Figure 8. (a) Target phase-velocity spectrum corresponding to the layer model in Table 1. (b) Best-matching phase-velocity spectrum from the inversion test on synthetic data. (c) The corresponding difference plot.

the material (Nazarian et al., 1999). Equation 7 is an approximation of the Rayleigh-wave equation and can be used to estimate a reference value of the shear-wave velocity from the measured $V_R$ and an assumed value of Poisson's ratio (Nazarian et al., 1999):

$$V_S = V_R(1.13 - 0.16\nu). \tag{7}$$

Equation 7 indicates that Poisson's ratio $\nu$ has an insignificant influence on the ratio between $V_R$ and $V_S$. Poisson's ratio is much more sensitive to the ratio between $V_P$ and $V_S$ and can be calculated by using

$$\nu = \frac{0.5(V_P/V_S)^2 - 1}{(V_P/V_S)^2 - 1}. \tag{8}$$

The estimated reference values of $\nu$ and $V_S$ (given in Table 2) have been calculated iteratively from the measured values of $V_R$ and $V_P$ by satisfying both equations 7 and 8. Similar measurements were made on top of each layer during pavement construction to obtain reference values from each layer. The measured $V_P$ and $V_S$ velocities from each layer, the given thickness, and the measured bulk density of each layer are presented in Table 2. Poisson's ratio of the second layer (base) is only 0.11. This agrees with laboratory acoustic measurements on granular materials (Santamarina et al., 2001). The asphalt material is viscoelastic, and this property by itself makes the seismic-wave propagation become dispersive. The dispersion becomes significant at high temperatures or low frequencies. Core samples of the asphalt layer were taken in the same section and tested in the laboratory. These measurements and the laboratory tests were carried out to obtain the best possible reference data for comparison with the results obtained from the inversion of all layers in the final pavement construction. However, $V_S$ of compacted pavement materials is sensitive to moisture content, aging effects, and the in-situ state of stress and consequently changes with time and climate (Santamarina et al., 2001). The inverted shear-wave velocities from the complete pavement construction should therefore not be expected to give exactly the same values as the reference shear-wave velocities measured on top of each layer.

Field data were acquired with only one accelerometer and a small hammer (Ryden et al., 2001, 2004), with offsets changing from 0.05–5.00 m in 0.05-m increments and using the equipment described in Ryden et al. (2002). A 40-ms record length and 200-kHz sampling rate were used. At each offset, recordings from four impacts delivered with a source-coupling device (a spike) were stacked vertically to result in one time series (one trace). The asphalt temperature was 13 °C. The compiled multichannel record is presented in Figure 10, and the corresponding phase-velocity spectrum is shown in Figure 11a. Three distinct mode branches are observed in the frequency range from 50–600 Hz.

To account for the viscoelastic properties, the shear-wave velocity of the asphalt layer was expressed during the inversion as a power law function of frequency

$$V_S(f) = b_1 f^{b_2}, \tag{9}$$

where $b_1$ and $b_2$ are coefficients to be determined through the inversion procedure. Material viscoelasticity affects wave propagation with a frequency-dependent stiffness (Young's modulus or velocity) and damping factor (Carcione, 1992). This simplified expression of stiffness as a function of frequency is possible because we are not utilizing the amplitude information in the measured data. The dynamic Young's modulus $E$ of the asphalt layer is usually represented by a master curve showing the dynamic modulus as a function of frequency at a reference temperature. Figure 12a shows the laboratory master curve at 13 °C obtained from the frequency sweep test (Uzan, 2003) made on core samples from the asphalt layer. Within the inversion frequency range (50–600 Hz), the dynamic modulus frequency relation is known to be close to linear on a log-log scale (Aouad, 1993), which motivates the chosen format of equation 9. The subsequent inversion then tries to solve for the viscoelastic constants ($b_1$ and $b_2$) rather than for a constant shear-wave velocity by assuming a

**Table 2. Pavement construction of a site in Malmoe, Sweden. Measured values (during construction) for thickness, shear-wave velocity, and compression-wave velocity are given, with results from the inversion of all layers in parenthesis.**

| Layer | $h$ (m) | $\nu$ | $\rho$ (kg/m$^3$) | $V_P$ (m/s) | $V_S$ (m/s) |
|---|---|---|---|---|---|
| 1. Asphalt | 0.130(0.129) | 0.30[1] | 2400[1] | | $880f^{0.070}$[1] ($888f^{0.059}$) |
| 2. Base | 0.300(0.308) | 0.11 | 2300 | 540 | 350 (371) |
| 3. Stab. subgr. | 0.200(0.203) | 0.20 | 2100 | 520 | 320 (368) |
| 4. Subgrade | >5.000 | 0.41 | 2100 | 550 | 213 (192) |

[1]Obtained from laboratory tests on core samples.

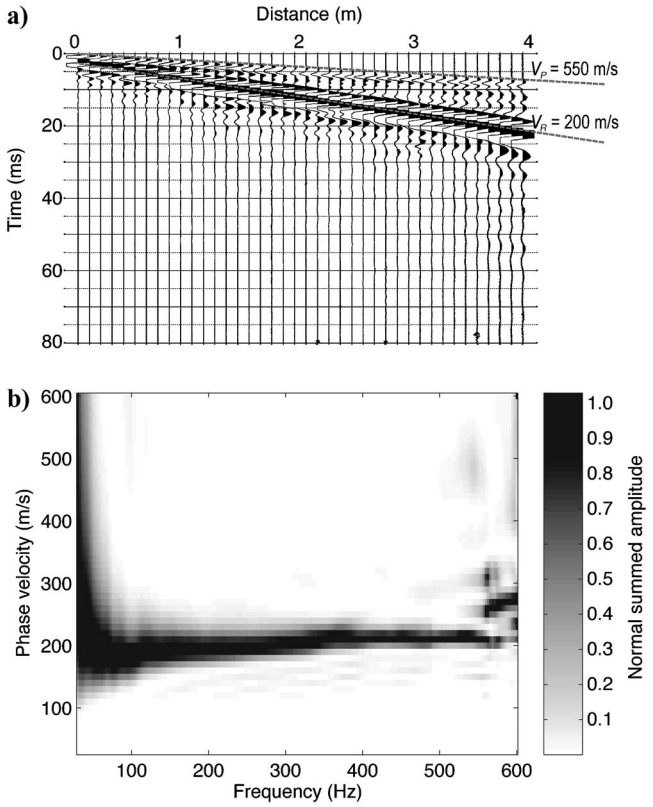


Figure 9. Field data from the Malmoe case study, with data recorded on top of the subgrade in (a) the time-offset domain and (b) the frequency–phase-velocity domain.

constant Poisson's ratio within this frequency range. Young's modulus is related to $V_S$ through

$$E = 2(\rho V_S^2)(1 + \nu). \quad (10)$$

The inversion algorithm was set up with the same settings used for the synthetic data example. The best-matching theoretical phase-velocity spectrum from the inversion is plotted in Figure 11b, and the difference plot is shown in Figure 11c. The corresponding layer model is presented in Table 2, where the parameters from the inversion are given in parentheses. Values of inversion parameters and their corresponding $M$ values from all iterations are plotted in Figure 13 within the predefined search range of each parameter (horizontal axis). The reference values from Table 2 are indicated with dashed lines in Figure 13. The inversion scheme was run for 800 transitions using 9106 trial layer models. Utilizing the described cooling schedule, the temperature and the corresponding perturbation size from the Cauchy distribution are so low after 800 transitions that it is not

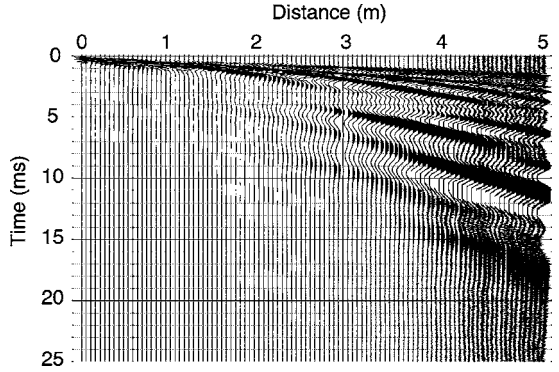


Figure 10. Field data from the Malmoe case study with data recorded on top of the final pavement construction (asphalt layer).

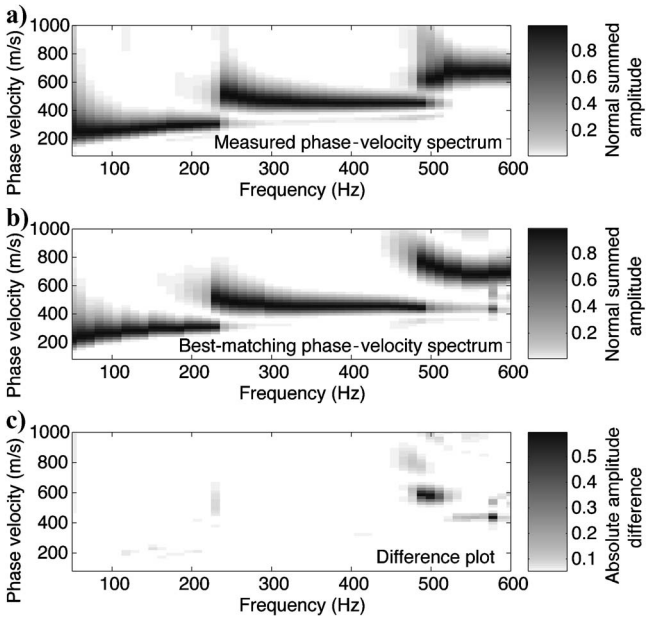


Figure 11. (a) Transformed phase-velocity spectrum from the recorded data in Figure 10. (b) Corresponding best-matching phase-velocity spectrum from the inversion. (c) The corresponding difference plot.

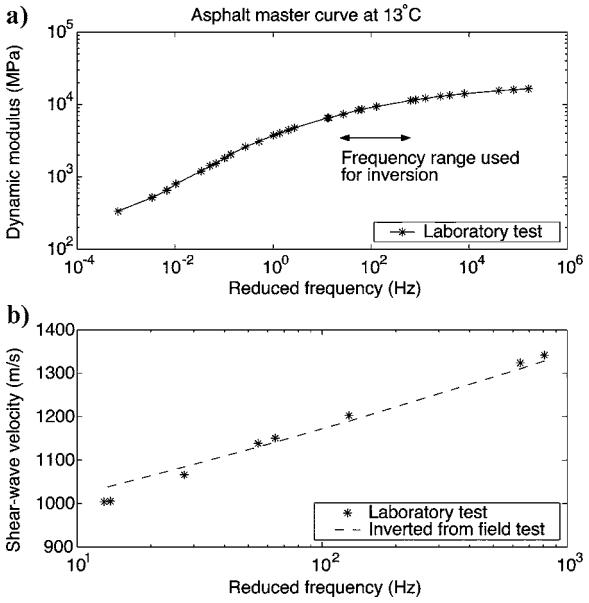


Figure 12. (a) Laboratory master curve from the Malmoe test site, showing the dynamic modulus of the asphalt layer as a function of frequency. (b) Corresponding laboratory and inverted shear-wave velocity within the frequency range used for the inversion.

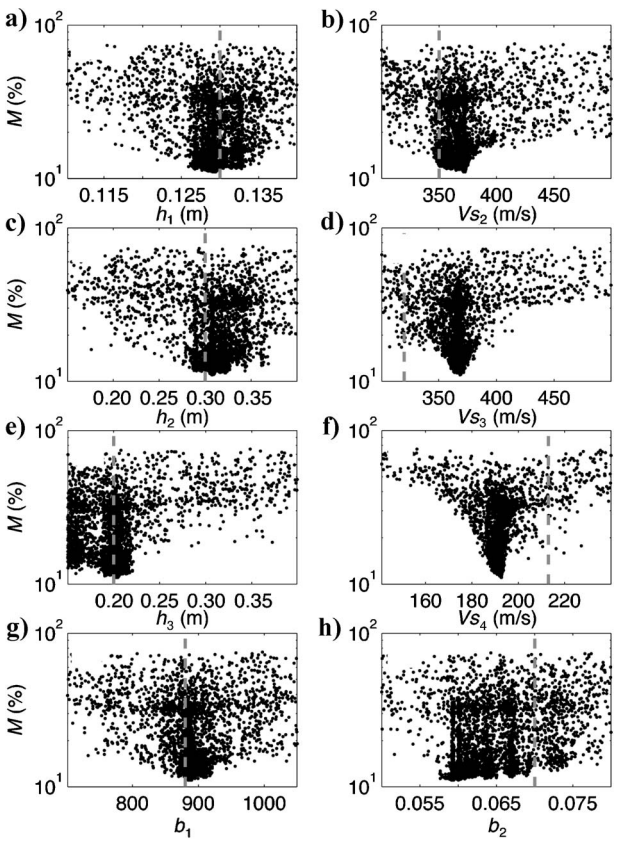


Figure 13. Mismatch $M$ as a function of parameter value from all iterations used in the FSA inversion of the field data example. The spread of the dots indicates the multidimensional sensitivity for each inverted parameter. Dashed lines indicate the reference values measured on each layer during pavement construction.

meaningful to continue the inversion. The total computational time was 3 hours using a 2.0-GHz PC.

Inverted parameters (Table 2) corresponding to an $M$ value of 9.1% agree quite well with the reference data (Table 2). Layer thicknesses are well resolved within 2.7% of the known thicknesses. The shear-wave velocity of the asphalt layer also agrees well with the results obtained from the laboratory test (Figure 12b). This indicates that the value of Young's modulus at 30 Hz, which is used in pavement engineering, can be obtained directly from the inverted shear-wave velocity of the asphalt layer. The shear-wave velocities of the base (371 m/s) and the stabilized subgrade (368 m/s) are slightly higher than the reference values. As mentioned earlier, the increase in stiffness can be explained by the higher confining pressure and the time difference (1–2 months) between the measurements of each layer and the final measurements on top of the asphalt layer. The inverted shear-wave velocity of the unstabilized subgrade (192 m/s) is 9.9% lower than the reference value (213 m/s) from Table 2. The shear-wave velocity of the subgrade (clay till) is more sensitive to changes in moisture content, which was not controlled during this test, compared to aging effects and the state of stress. The relatively large discrepancy for this parameter may also be explained from the relatively low sensitivity (wide valley) shown in Figure 4.

## DISCUSSION

FSA of the complete phase-velocity spectrum is computationally more demanding than conventional least-squares inversion of discrete dispersion curves. However, the increased computational time can be justified by the robustness of FSA because raw field data can be inverted without any subjective user input to identify discrete dispersion curves and with a minimum risk of getting trapped in a local minimum. Potential drawbacks of FSA are related to the SA control parameters governing the cooling schedule and the perturbation size and range of each parameter to be inverted. The frequency range and sampling (e.g., linear, logarithmic, or other) also affect the sensitivity of the inverted parameters. A frequency range with good S/N ratio (clear dispersion-curve trends) should be used. These parameters need to be set subjectively for each type of application. Other inherent limitations can be related to the use of perfectly homogeneous, elastic, or viscoelastic flat layers in the forward model. FSA is only one of several global optimization methods; other methods may be worth testing (see, for example, Mosegaard and Sambridge, 2002).

The difference in the final result between the proposed approach and the conventional least-squares inversion of discrete dispersion curves depends heavily on the complexity of the data, i.e, layer model. In situations where the measured dispersion curve and corresponding mode number can be identified easily, it may be more efficient to use the conventional inversion procedure with many different starting models. However, in many cases mode-number identification and separation are impossible; this is when FSA has the biggest advantage over the conventional method.

Our method focuses on the inversion utilizing the phase-velocity spectrum only, with the objective function defined solely by the characteristics of the phase-velocity spectrum. However, this function can be completely user defined and optimized for each specific application. For example, higher frequencies and first-arrival velocities can be included in the objective function for surface-wave testing of pavement. This will introduce some additional constraints on the properties of the top layer. Future developments may include some quantification of the uncertainty of the inverted parameter values.

While this study focuses on the inversion of pavement layer properties, the same procedure can be used for the inversion of surface-wave data from any type of layered half-space or plate. Other applications may include inversion of surface-wave data from soil sites or in the field of ultrasonic testing of composite plates and coatings.

## CONCLUSIONS

An alternative inversion scheme using FSA to invert the complete phase-velocity spectrum of surface waves has been presented. This method is less likely to get trapped in local minima, and it is not dependent on dispersion curve picking, mode-number identification, or partial derivatives for the inversion. Once the FSA control parameters are set up, the raw field data can be processed and inverted to a shear-wave velocity layer model without further subjective user input and by properly accounting for the interference of different modes and types of waves. This is a significant advantage when surface-wave data involve multiple modes of propagation. The main disadvantage at this point is the large amount of computational time required for the inversion process compared to the traditional gradient-based inversion of surface-wave dispersion curves.

The viscoelastic properties of the asphalt layer are included in the forward model, resulting in an inverted master curve that shows asphalt stiffness as a function of frequency. With this procedure the dynamic asphalt modulus at 30 Hz, used in pavement engineering, can be estimated directly from surface-wave tests without further reduction factors.

It seems that the resolution of the base layer (which has been a challenging task with traditional methods) can be improved with our method. This improvement in resolution is obtained using the full phase-velocity spectrum in the inversion method. Compared to the conventional approach, where only one apparent dispersion curve is used, this utilization is believed to reduce the amount of nonuniqueness.

## ACKNOWLEDGMENTS

We sincerely thank Peab, VINNOVA, and the Swedish National Road Administration for financing this project. We also thank Nenad Gucunski at Rutgers University for his assistance with the stiffness matrix method. Help from Mary Brohammer and Marla Adkins-Heljeson with the preparation of this manuscript is also greatly appreciated.

## REFERENCES

Abdallah, I., D. Yuan, and S. Nazarian, 2003, Validation of software developed for determining design modulus from seismic testing: University of Texas at El Paso Center for Highway Materials Research, Research Report 1780-5.

Akhlaghi, B. T., and W. H. Cogill, 1994, Application of the free plate analogy to a single-layered pavement system: Insight, **36**, 514–518.

Andresen, B., and J. M. Gordon, 1994, Constant thermodynamic speed for minimizing entropy production in thermodynamic processes and simulated annealing: Physical Review E, **50**, 4346–4351.

Aouad, M. F., 1993, Evaluation of flexible pavements and subgrades using the spectral-analysis-of-surface-waves (SASW) method: Ph.D. thesis, University of Texas.

Basu, A., and L. N. Frazer, 1990, Rapid determination of the critical temperature in simulated annealing inversion: Science, **249**, 1409–1412.

Beaty, K. S., and D. R. Schmitt, 2003, Repeatability of multimode Rayleigh-

wave dispersion studies: Geophysics, **68**, 782–790.
Beaty, K. S., D. R. Schmitt, and M. Sacchi, 2002, Simulated annealing inversion of multimode Rayleigh wave dispersion curves for geological structure: Geophysical Journal International, **151**, 622–631.
Carcione, J. M., 1992, Rayleigh waves in isotropic viscoelastic media: Geophysical Journal International, **108**, 453–464.
Dal Moro, G., M. Pipan, E. Forte, and I. Finetti, 2003, Determination of Rayleigh wave dispersion curves for near surface applications in unconsolidated sediments: 73rd Annual International Meeting, SEG, Expanded Abstracts, 1247–1250.
Dosso, S. E., M. J. Wilmut, and A.-L. S. Lapinski, 2001, An adaptive-hybrid algorithm for geoacoustic inversion: IEEE Journal of Oceanic Engineering, **26**, 324–336.
Ekdahl, U., P. E. Bengtsson, and N. Ryden, 2004, A new framework for analytical pavement design based on systematic control during construction work: Proceedings of the 14th Nordic Geotechnical Meeting, E55–E80.
Forbriger, T., 2003, Inversion of shallow-seismic wavefields, part 2: Inferring subsurface properties from wavefield transforms: Geophysical Journal International, **153**, 719–734.
Foti, S., L. Sambuelli, V. L. Socco, and C. Strobbia, 2003, Experiments of joint acquisition of seismic refraction and surface wave data: Near Surface Geophysics, **1**, 119–129.
Gabriels, P., R. Snieder, and G. Nolet, 1987, In situ measurements of shear-wave velocity in sediments with higher-mode Rayleigh waves: Geophysical Prospecting, **35**, 187–196.
Ganji, V., N. Gucunski, and S. Nazarian, 1998, Automated inversion procedure for spectral analysis of surface waves: Journal of Geotechnical and Geoenvironmental Engineering, **124**, 757–770.
Gucunski, N., I. N. Abdallah, and S. Nazarian, 2000, ANN backcalculation of pavement profiles from the SASW test, in Pavement subgrade unbound materials, and nondestructive testing: ASCE Geotechnical Special Publication 98, 31–50.
Gucunski, N., and A. Maher, 2000, Evaluation of the dynamic response of pavements and other layered systems using the stiffness matrix approach: Proceedings of the 79th Annual Meeting, Transportation Research Board, 00-0134.
Gucunski, N., and R. D. Woods, 1992, Numerical simulation of the SASW test: Soil Dynamics and Earthquake Engineering, **11**, 213–227.
Hadidi, R., and N. Gucunski, 2003, Inversion of SASW dispersion curve using numerical simulation: Proceedings of the Symposium on the Application of Geophysics to Engineering and Environmental Problems (SAGEEP 2003), SUR-01.
Haegeman, W., 2002, In situ assessment of stiffness of a road sand embankment: Proceedings of the Conference on Bearing Capacity of Roads, Railways, and Airfields, 629–635.
Haskell, N. A., 1953, The dispersion of surface waves on multilayered media: Bulletin of the Seismological Society of America, **43**, 17–34.
Heisey, J. S., K. H. Stokoe, and A. H. Meyer, 1982, Moduli of pavement systems from spectral analysis of surface waves: Transportation Research Record, **852**, 22–31.
Hoffmann, K. H., and P. Salamon, 1990, The optimal simulated annealing schedule for a simple model: Journal of Physics A: Mathematical and General, **23**, 3511–3523.
Jones, R., 1962, Surface wave technique for measuring the elastic properties and thickness of roads: Theoretical development: British Journal of Applied Physics, **13**, 21–29.
Kausel, E., and J. M. Roësset, 1981, Stiffness matrices for layered soils: Bulletin of the Seismological Society of America, **71**, 1743–1761.
Kirkpatrick, S., C. D. Gelatt, Jr., and M. P. Vecchi, 1983, Optimization by simulated annealing: Science, **220**, 671–680.
Laarhoven, P. J. M., and E. H. L. Aarts, 1987, Simulated annealing: Theory and applications: Kluwer Academic Publishers.
Martínez, M. D., X. Lana, J. Olarte, J. Badal, and J. A. Canas, 2000, Inversion of Rayleigh wave phase and group velocities by simulating annealing: Physics of the Earth and Planetary Interiors, **122**, 3–17.
Menke, W., 1989, Geophysical data analysis: Discrete inverse theory, revised ed.: Academic Press.
Mosegaard, K., and M. Sambridge, 2002, Monte Carlo analysis of inverse problems: Inverse Problems, **18**, R29–R54.
Nazarian, S., 1984, In situ determination of soil deposits and pavement systems by spectral analysis of surface waves method: Ph.D. thesis, University of Texas.
Nazarian, S., D. Yuan, and V. Tandon, 1999, Structural field testing of flexible pavement layers with seismic methods for quality control: Transportation Research Record, **1654**, 50–60.
Park, C., R. D. Miller, and J. Xia, 1998, Imaging dispersion curves of surface waves on multichannel records: 68th Annual International Meeting, SEG, Expanded Abstracts, 1377–1380.
———, 1999, Multichannel analysis of surface waves: Geophysics, **64**, 800–808.
———, 2001, Offset and resolution of dispersion curve in multichannel analysis of surface waves (MASW): Proceedings of the Symposium on the Application of Geophysics to Engineering and Environmental Problems (SAGEEP 2001), SSM-4.
Roësset, J. M., D. W. Chang, K. H. Stokoe II, and M. Auoad, 1990, Modulus and thickness of the pavement surface layer from SASW tests: Transportation Research Record, **1260**, 53–63.
Ryden, N., and M. J. S. Lowe, 2004, Guided wave propagation in three-layer pavement Structures: Journal of the Acoustical Society of America, **116**, 2902–2913.
Ryden, N., and C. B. Park, 2004, Surface waves in inversely dispersive media: Near Surface Geophysics, **2**, 187–197.
Ryden, N., C. B. Park, P. Ulriksen, and R. D. Miller, 2004, Multimodal approach to seismic pavement testing: Journal of Geotechnical and Geoenvironmental Engineering, **130**, 636–645.
Ryden, N., P. Ulriksen, C. B. Park, and R. D. Miller, 2002, Portable seismic acquisition system (PSAS) for pavement MASW: Proceedings of the Symposium on the Application of Geophysics to Engineering and Environmental Problems (SAGEEP 2002), 13IDA7.
Ryden, N., P. Ulriksen, C. B. Park, R. D. Miller, J. Xia, and J. Ivanov, 2001, High frequency MASW for non-destructive testing of pavements-accelerometer approach: Proceedings of the Symposium on the Application of Geophysics to Engineering and Environmental Problems (SAGEEP 2001), RBA-5.
Sambridge, M., 1999, Geophysical inversion with a neighbourhood algorithm I: Searching a parameter space: Geophysical Journal International, **138**, 479–494.
Santamarina, J. C., K. A. Klein, and M. A. Fam, 2001, Soils and waves: John Wiley & Sons.
Sen, M., and P. L. Stoffa, 1995, Global optimization methods in geophysical inversion: Elsevier Science Publishing Co.
Socco, L. V., C. Strobbia, and S. Foti, 2002, Multimodal interpretation of surface wave data: Proceedings of the 8th Annual Meeting, Environmental and Engineering Geophysical Society European Section, 21–25.
Stokoe, K. H., II, S. G. Wright, J. A. Bay, and J. M. Roësset, 1994, Characterization of geotechnical sites by SASW method, *in* R. D. Woods, ed., Geophysical characterization of sites: ISSMFE Technical Committee Report 10: Oxford Publishers.
Szu, H., and R. Hartley, 1987, Fast simulated annealing: Physics Letters A, **122**, 157–162.
Thomson, W. T., 1950, Transmission of elastic waves through a stratified solid medium: Journal of Applied Physics, **21**, 89–93.
Uzan, J., 2003, Characterization of asphalt concrete materials for permanent deformation, International Journal of Pavement Engineering, **4**, 77–86.
Van der Poel C., 1951, Dynamic testing of road constructions, Journal of Applied Chemistry, **1**, 281–290.
Vidale, R. F., 1964, The dispersion of stress waves in layered media overlaying a half space of lesser acoustic rigidity: Ph.D. thesis, University of Wisconsin.
Wu, H., S. Wang, I. Abdallah, and S. Nazarian 2002, A rapid approach to interpretation of SASW results: Proceedings of the Conference on Bearing Capacity of Roads, Railways, and Airfields, 761–770.
Xia, J., R. D. Miller, and C. B. Park, 1999, Estimation of near-surface shear-wave velocity by inversion of Rayleigh waves: Geophysics, **64**, 691–700.
Zhang, S. X., and L. S. Chan, 2003, Possible effects of misidentified mode number on Rayleigh wave inversion: Journal of Applied Geophysics, **53**, 17–29.
Zywicki, D. J., 1999, Advanced signal processing methods applied to engineering analysis of seismic surface waves: Ph.D. thesis, Georgia Institute of Technology.